Mixed Finite-Difference, Finite Volume Implicit TVD Scheme for Computation of Transonic Flows

A. Sedaghat*, **S. Shahpar**†, **I. M. Hall**‡
The Manchester School of Engineering
Aerospace Engineering Division, Oxford Road
Manchester M13 9PL
UK

ABSTRACT. A parametric study has been conducted to assess the performance of a mixed finite-difference, finite-volume implicit TVD scheme initially proposed by Yee. The new scheme has reduced dependency of final results on some parameters such as grid resolution, correction of limiters on boundaries, and also the type of local time-stepping used. Furthermore, about 40% run-time saving is achieved for most test cases considered here. Viscous flows have been computed for the RAE2822 aerofoil using Baldwin-Lomax turbulent model. The results are compared with other experimental and numerical results.

KEY WORDS: TVD Algorithms, Supercritical Aerofoils, Turbulent Flows.

1. Introduction

A number of new techniques for constructing non-linear, high-resolution shock-capturing schemes for systems of hyperbolic conservation laws have been developed. These schemes, characterized by the Total Variation Diminishing (TVD) property, are free from generating spurious oscillations across the regions of sharp flow profiles such as shocks and contact discontinuities. These methods require an entropy correction to converge to physically meaningful solutions. In the region of smoothly varying solutions the TVD schemes can

*Research student
†Research fellow in Aerospace Engineering
‡Senior lecturer in Aerospace Engineering

also maintain a high degree of numerical accuracy.

The TVD concept was first proposed by Harten for first-order schemes. Later, Harten (1983) constructed a second-order TVD scheme by adding a limited antidiffusive flux to a first-order scheme. Harten also extended a class of explicit TVD schemes to a more general category which includes a one-parameter family of implicit second-order TVD schemes. Harten's TVD scheme was modified and generalized by Yee (1986) and implemented to solve the two-dimensional Euler equations of gas-dynamics for the aerofoil problem.

In the present study, the finite-difference explicit part in Yee's implicit scheme has been replaced by a cell-vertex finite-volume scheme and some terms in the implicit part and TVD dissipation functions are also modified. Since at steady-state the solution of implicit schemes converge to the explicit part by vanishing the implicit part, we can claim that the final results are truly based on a finite-volume scheme which is mostly desirable for aerofoil flows. Therefore, the similar codes in general coordinates can easily be modified by this approach. The derivation of this class of TVD schemes in two-dimensional generalized curvilinear coordinates and the details of the scheme for solving full compressible Navier-Stokes equations are presented.

The goal is to assess the performance of this scheme in terms of numerical accuracy, robustness and convergence rate. The best results corresponding to the upwind TVD scheme using the Van-Leer limiter are presented here.

2. Governing Equations

The nondimensional form of the compressible Navier-Stokes equations in general curvilinear coordinates in two dimensions is

$$\frac{\partial \hat{\mathbf{U}}}{\partial t} + \frac{\partial \hat{\mathbf{F}}}{\partial \xi} + \frac{\partial \hat{\mathbf{G}}}{\partial \eta} = 0 \tag{1}$$

$$\begin{aligned} \hat{\mathbf{U}} &= \mathbf{U}/J \\ \hat{\mathbf{F}} &= (\xi_x \mathbf{F} + \xi_y \mathbf{G})/J \quad , \quad \hat{\mathbf{G}} = (\eta_x \mathbf{F} + \eta_y \mathbf{G})/J \\ J &= \xi_x \eta_y - \xi_y \eta_x \end{aligned} \tag{2}$$

where $\xi = \xi(x, y)$, $\eta = \eta(x, y)$ are coordinate transformation functions and J is the Jacobian of the transformation. $\mathbf{U}$, $\mathbf{F}$, and $\mathbf{G}$ are vectors of conservative variables and fluxes, respectively.

3. The Numerical Algorithm

The Alternative Direction Implicit (ADI) form of the Linearized Conservative Implicit (LCI) of Yee's (1988) TVD scheme in generalized curvilinear

coordinates can be written as

$$\begin{aligned}\{\mathbf{I}+\Delta t_{ij}\ (\mathbf{H}^{\xi}_{i+1/2,j}-\mathbf{H}^{\xi}_{i-1/2,j})\}\frac{\mathbf{E}^*}{J} &= \frac{\mathbf{RHS}}{J}\\ \{\mathbf{I}+\Delta t_{ij}\ (\mathbf{H}^{\eta}_{i,j+1/2}-\mathbf{H}^{\eta}_{i,j-1/2})\}\frac{\mathbf{E}^n}{J} &= \frac{\mathbf{E}^*}{J}\end{aligned} \tag{3}$$

with $\mathbf{U}^{n+1}=\mathbf{U}^n+\mathbf{E}^n$. The operators $\mathbf{H}^{\xi}$ and $\mathbf{H}^{\eta}$ are defined as

$$\begin{aligned}\mathbf{H}^{\xi}_{i\pm1/2,j}\mathbf{E}^* &= \frac{1}{2}[\hat{\mathbf{A}}_{i\pm1,j}\mathbf{E}^*_{i\pm1,j}-\mathbf{\Omega}^{\xi}_{i\pm1/2,j}\mathbf{E}^*]\\ \mathbf{H}^{\eta}_{i,j\pm1/2}\mathbf{E}^n &= \frac{1}{2}[\hat{\mathbf{B}}_{i,j\pm1}\mathbf{E}^n_{i,j\pm1}-\mathbf{\Omega}^{\eta}_{i,j\pm1/2}\mathbf{E}^n]\end{aligned} \tag{4}$$

The Jacobian matrices $\hat{\mathbf{A}}$ and $\hat{\mathbf{B}}$ result from the linearization of the flux vectors $\hat{\mathbf{F}}$ and $\hat{\mathbf{G}}$ respectively.

For steady-state applications

$$\begin{aligned}\mathbf{\Omega}^{\xi}_{i+1/2,j}\mathbf{E}^* &= M^{\xi}_{i+1/2,j}\mathbf{I}(\mathbf{E}^*_{i+1,j}-\mathbf{E}^*_{i,j})\\ \mathbf{\Omega}^{\eta}_{i,j+1/2}\mathbf{E}^n &= M^{\eta}_{i,j+1/2}\mathbf{I}(\mathbf{E}^n_{i,j+1}-\mathbf{E}^n_{i,j})\end{aligned} \tag{5}$$

The scalar values M^{ξ} and M^{η} are

$$\begin{aligned}M^{\xi}_{i+1/2,j} &= max[\psi(a^l_{i+1/2})]\\ M^{\eta}_{i,j+1/2} &= max[\psi(a^l_{j+1/2})]\end{aligned} \tag{6}$$

where I, $a^l_{i+1/2}$ and $a^l_{j+1/2}$, and ψ are (4×4) identity matrix, the eigenvalues correspond to the $\hat{\mathbf{A}}$ and $\hat{\mathbf{B}}$, and entropy correction function, respectively. The **RHS** here is a combination of a cell-vertex finite-volume approach of Fletcher (1988) and the numerical dissipation of the Yee's TVD scheme as:

$$\begin{aligned}\mathbf{RHS} &= -\frac{\Delta t_{i,j}}{A_{i,j}}\sum_{AB}^{DA}(\mathbf{F}\Delta y-\mathbf{G}\Delta x)\\ &- \frac{\Delta t_{i,j}}{2}[(\mathbf{R}_{i+1/2,j}\mathbf{\Phi}_{i+1/2,j}-\mathbf{R}_{i-1/2,j}\mathbf{\Phi}_{i-1/2,j})\\ &+ (\mathbf{R}_{i,j+1/2}\mathbf{\Phi}_{i,j+1/2}-\mathbf{R}_{i,j-1/2}\mathbf{\Phi}_{i,j-1/2})]\end{aligned} \tag{7}$$

$(\phi^l_{i+1/2})^U$ for the second-order upwind TVD scheme are as follows

$$(\phi^l_{i+1/2})^U=\frac{1}{2}\psi(a^l_{i+1/2})(g^l_{i+1}+g^l_i)\psi(a^l_{i+1/2}+\gamma^l_{i+1/2})\alpha^l_{i+1/2} \tag{8}$$

with the functions γ and ψ defined as

$$\gamma^l_{i+1/2}=\frac{1}{2}\psi(a^l_{i+1/2})\begin{cases}(g^l_{i+1}-g^l_i)/\alpha^l_{i+1/2} & \alpha^l_{i+1/2}\neq0\\ 0 & \alpha^l_{i+1/2}=0\end{cases} \tag{9}$$

$$\psi(z) = \begin{cases} |z| & |z| \geq \epsilon \\ (z^2 + \epsilon^2)/2\epsilon & |z| < \epsilon \end{cases} \tag{10}$$

with $\epsilon = 0.125$. The characteristic function $\alpha^l_{i+1/2}$ is defined as

$$\alpha^l_{i+1/2} = \mathbf{R}^{-1}_{i+1/2}(\mathbf{U}_{i+1} - \mathbf{U}_i) \tag{11}$$

with $\mathbf{R}$ is right eigenvector matrix, see Sedaghat (1993).

In all test cases, the Van-Leer limiter function $g^l_{i+1/2}$ is used and is given by

$$\begin{aligned} g^l_i &= \{\alpha^l_{i-1/2}[(\alpha^l_{i+1/2})^2 + \delta] + \alpha^l_{i+1/2}[(\alpha^l_{i-1/2})^2 + \delta]\} \\ &\quad /[(\alpha^l_{i+1/2})^2 + (\alpha^l_{i-1/2})^2 + 2\delta] \end{aligned} \tag{12}$$

with δ a small parameter ($10^{-7} \leq \delta \leq 10^{-5}$). In all the above equations Roe's (1981) averaging is used to evaluate $\mathbf{U}_{i+1/2}$ and corresponding terms.

4. Results and Discussion

In this section, results are presented for the RAE 2822 aerofoil covering a range of conditions from fully subcritical flow to supercritical flow with shock-induced separation. The calculations are carried out using the method with a fixed set of flow algorithm and grid generation parameters.

Computational grids are constructed using the algebraic grid generator of Rizzi (1981) together with a hyperbolic grid generator of Alsalihi (1987) to produce an orthogonal C-mesh for the test cases (see Fig. 1). A relatively coarse mesh of 141×61 has been used in order to investigate the performance of the numerical algorithm. The outer boundary is placed at 18 chord lengths away from the aerofoil surface. The first cell-size at both the leading edge and the trailing edge is fixed as $\frac{\Delta\xi}{c} = 0.002$ and $\frac{\Delta\eta}{c} = 0.00002$. In the wake region 24×61 grid points have been placed between the upper and the lower wake cut. The outflow boundary is placed 10 chords length downstream of the trailing edge.

Each test case was initialized by uniform freestream conditions at a prescribed Mach number and angle of attack. The no-slip condition together with zero normal pressure gradient and zero normal temperature gradient (adiabatic wall) have been applied on the aerofoil surface. The characteristic boundary condition, given by Jameson (1983), has been used for the outer boundary and zero-extrapolation was used for the outflow boundary. Across the wake region, all conservative variables have been averaged.

A local time-stepping based on mesh Jacobians is used here as follows

$$\Delta t_{i,j} = \frac{T}{1 + \sqrt{J_{i,j}}} \tag{13}$$

where T is a constant, to provide the maximum allowed time-step. A typical value of 0.5 is used for T in current computations.

An experimental study of RAE 2822 aerofoil in the 8ft $\times$ 6ft transonic wind tunnel at RAE Farnborough was presented by Cook et al (1979). Their measurement data has been used extensively to validate numerical methods, see Holst (1988).

Figure 1 shows the RAE 2822 aerofoil with a close-up of the computational grid. Four cases are considered here and the relevant flow conditions are given in Table 1(a). Comparisons of predicted and measured lift, drag and pitching moment coefficients and also Johnston's (1991) numerical results are shown in Table 1(b). Note that Johnston's results are based on a fairly fine mesh consisting of 272 $\times$ 64 cells. Transition is fixed at 11 % chord for Case 1 and at 3 % chord for the others on the upper and lower surfaces of the aerofoil.

Case 6 presents a supercritical flow on the upper surface terminated by a shock wave of moderate strength just downstream of the mid-chord position. Drag and moment coefficients predicted by present method are in good agreement with measurements. However, the predicted lift coefficient is a little higher than the available data. Similarly, as shown in Figure 2, the shock wave is predicted to be a little too far upstream. This is in agreement with other calculation methods; see Johnston (1991), and Holst (1988) for example. This simple algebraic turbulence model is believed to be the cause of this discrepancies in the shock wave position. Very good agreement in skin friction is achieved upstream of the shock wave, but relatively poor prediction is observed downstream of the shock wave which results from the discrepancies in shock wave position. The convergence of the drag coefficient is found to be rapid.

For Case 9, aerodynamic coefficients match closely with the measurements. In Figure 3, better agreement in shock wave position is observed, as has also reported by Johnston. The upper surface skin friction distribution, in Figure 4(b), indicates flow separation at the foot of the shock wave for the Baldwin-Lomax (1978) turbulent model. No separation in the experiment was reported for this case by Cook (1979). This tendency of the Baldwin-Lomax model to predict premature flow separation, particularly in the shock wave position, has been noted by other authors, see Holst (1988). Similar convergence with the other test cases is observed.

5. Conclusion

In the initial phase of this study, a fast algorithm utilizing a modified upwind, implicit, Total Variation Diminishing (TVD) scheme has been developed. Viscous, turbulent, transonic flows over aerofoils have been studied. A hyperbolic C-mesh has been used to provide an orthogonal grid around the aerofoil section. This study has shown that aerodynamic coefficients can be predicted more accurately with the new scheme using a relatively coarse orthogonal grid. As a consequence of the good drag prediction ability of this method, drag

reduction techniques can also be investigated which is the subject of current research.

6. Bibliography

[ALS 87] Alsalihi, Z., "Two Dimensional Hyperbolic Grid Generation", *Von Kar man Institute for Fluid Dynamics, Technical Note 162*, October 1987.

[BAL 78] Baldwin, B. and Lomax, H., "Thin Layer Approximation and Algebraic Model for Separated Turbulent Flows", *AIAA Paper No. 78-257*, 1978.

[COO 79] Cook, P. H., McDonald, M. A., and Firmin, M. C. P., "Aerofoil RAE 2822 - Pressure Distribution, and Boundary Layer and Wake Measurements", *AGARD AR 138*, Paper A6, May 1979.

[FLE 88] Fletcher, C. A. J., "Computational Techniques for Fluid Dynamics", *Springer - Verlag*, 1988.

[HAR 83] Harten A., "A High Resolution Scheme for the Computation of Weak So lutions of Hyperbolic Conservation Laws", *J. Comp. Phys.* , 49, p. 357-393, 1983.

[HOL 88] Holst, T. L., "Viscous Transonic Airfoil Workshop Compendium of Results" , *AIAA Paper No. 87-1460*, 1987; *J. Aircraft*, Vol. 25, No. 12, pp. 1073-1087, 1988.

[JAM 83] Jameson, A. and Baker, T. J., "Solution of the Euler Equations for Com plex Configurations", *AIAA Paper No. 83-1929*, 1983.

[JOH 91] Johnston, L. J., "Solution of the Reynolds-Averaged Navier-Stokes Equa tions for Transonic Aerofoil Flows", *Aeronautical J.*, pp. 253-273, 1991.

[RIZ 81] Rizzi, A. and Vivand H., "Numerical Methods for the Computation of Inviscid Transonic Flows with Shock Waves", *Notes on Numerical Fluid Mechan ics*, Vol 3, Vieweg, 1981.

[ROE 81] Roe, P. L., "Approximate Riemann Solvers, Parameter Vectors, and Dif ference Schemes", *J. Comp. Phys.*, Vol. 43, pp. 357-372, 1981.

[SED 93] Sedaghat, A, "Comparative Study of High-Resolution Shock-Capturing Schemes for External Supersonic Flows", *MSc thesis*, Manchester University, 1993.

[YEE 86] Yee, H. C. and Harten A., "Implicit TVD Schemes for Hyperbolic Con servation Laws in Curvilinear Coordinates", *AIAA J.*, Vol. 25, No. 2, pp. 226-274, 1986.

[YEE 88] Yee, H. C., Klopfer, G. H. and Montagne, J. L. "High-Resolution Shock -Capturing Schemes for Inviscid and Viscous Hypersonic Flows", *NASA TM-100097*, April 1988.

TABLE 1
RAE 2822 Aerofoil
Results using Baldwin-Lomax (B-L) model
(a) Flow conditions

Case	M	α	$R_e \times 10^{-6}$
1	0.676	1.93^o	5.7
6	0.725	2.54^o	6.5
9	0.730	2.79^o	6.5
10	0.750	2.81^o	6.2

b) Comparison of measured and calculated loads

Case 1	C_L	C_D	$C_M(1/4)$
Experiment	0.566	0.0085	-0.082
Johnston (B-L)	0.5802	0.01068	-0.08769
present (B-L)	0.5750	0.0084	-0.08593

Case 6	C_L	C_D	$C_M(1/4)$
Experiment	0.743	0.0127	-0.095
Johnston (B-L)	0.7457	0.01502	-0.09175
present (B-L)	0.7637	0.01199	-0.09255

Case 9	C_L	C_D	$C_M(1/4)$
Experiment	0.803	0.0168	-0.099
Johnston (B-L)	0.7950	0.01884	-0.09513
present (B-L)	0.8174	0.01593	-0.09642

Case 10	C_L	C_D	$C_M(1/4)$
Experiment	0.743	0.0242	-0.106
Johnston (B-L)	0.7901	0.02921	-0.1108
present (B-L)	0.8157	0.02582	-0.1117

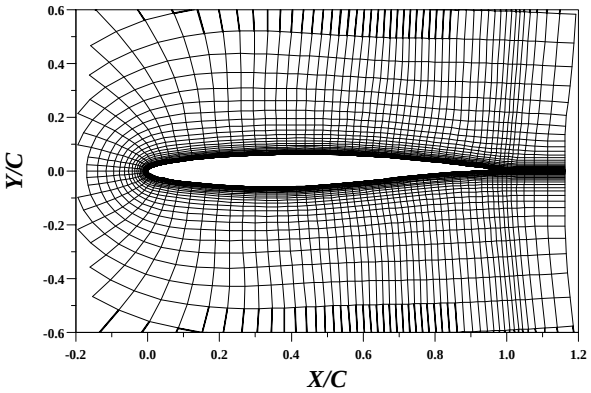

Figure 1: A sectional view of the C-hyperbolic mesh generated around the RAE 2822 aerofoli.

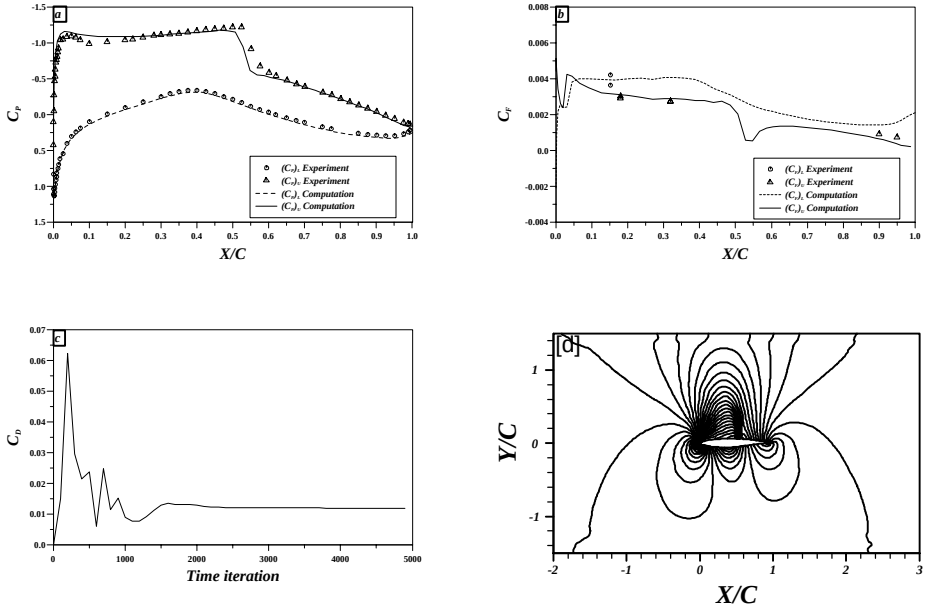

Figure 2: Results for the RAE 2822 aerofoil (case 6), $M = 0.725$, $\alpha = 2.54^o$, $Re = 6.5 \times 10^6$. a) surface pressure coefficient, b)surface skin friction coefficient, c) drag convergence, and d) pressure contours.

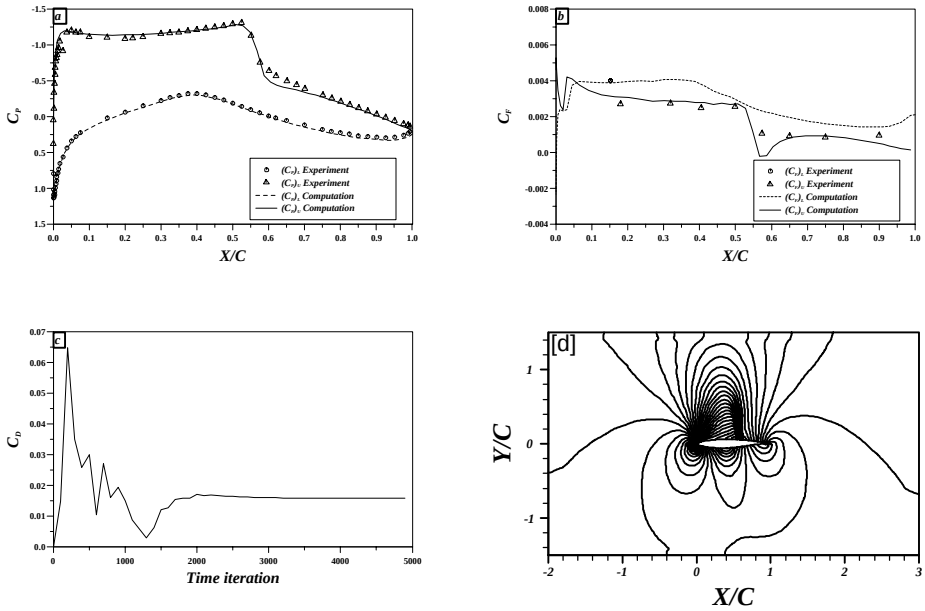

Figure 3: Results for the RAE 2822 aerofoil (case 9), $M = 0.73$, $\alpha = 2.79^o$, $Re = 6.5 \times 10^6$. a) surface pressure coefficient, b)surface skin friction coefficient, c) drag convergence, and d) pressure contours.